Eccentricity estimation from initial data for numerical relativity simulations

Alessandro Ciarfella,[1] James Healy,[1] Carlos O. Lousto,[1] and Hiroyuki Nakano[2]
[1]*Center for Computational Relativity and Gravitation, School of Mathematical Sciences, Rochester Institute of Technology, 85 Lomb Memorial Drive, Rochester, New York 14623, USA*
[2]*Faculty of Law, Ryukoku University, Kyoto 612-8577, Japan*

(Received 27 June 2022; revised 21 September 2022; accepted 24 October 2022; published 16 November 2022)

We describe and study an instantaneous definition of eccentricity to be applied at the initial moment of full numerical simulations of binary black holes. The method consists of evaluating the eccentricity at the moment of maximum separation of the binary. We estimate it using up to third post-Newtonian (3PN) order and compare these estimates with the results of evolving (conservative) 3PN equations of motion for a full orbit and compute the eccentricity e_r from the radial turning points, finding excellent agreement. We then include terms with spins up to 3.5PN and next compare this initial data eccentricity estimate method with the turning points estimates of the eccentricity e_r^{NR} during full numerical evolutions of spinning binary black holes, characterized invariantly by a fractional factor $0 \leq f \leq 1$ of the initial tangential momenta to a quasicircular one. We find that our initial instantaneous definition is a particularly useful and accurate tool to predict and characterize even highly eccentric full numerical simulations.

DOI: 10.1103/PhysRevD.106.104035

I. INTRODUCTION

While the concept of eccentricity is uniquely defined in Newtonian gravity, an extension to general relativity is not strictly uniquely or even well defined, but we have found it useful to have an instantaneous eccentricity estimate e defined at the initial data level of a full numerical simulation. The question of astrophysical binary black holes retaining non-negligible eccentricity close to merger has been the subject of recent interest [1–3], with growing observational evidence from gravitational wave events that large eccentricities may actually occur in nature [4–8].

To start a full numerical simulation of a binary black hole, we have to choose first the orbital parameters at the beginning of the simulation, then compute the initial data (metric variables and its first time derivatives) along with choices of gauge and numerical coordinates to perform the desired evolution [9]. To compute the numerical initial data, we use the puncture approach [10] along with the TWOPUNCTURES [11] code implementation. For each eccentric family of simulations, we first determine at the initial separation R_c the tangential quasicircular momentum P_c, using the results of [12]. To increase the eccentricity of the system at an apocenter, the initial tangential momentum P_t is modified by a fractional parameter $0 \leq f \leq 1$, such that $P_t = (1-f)P_c$. See Fig. 1 for a schematic representation.

This method was applied to the estimates of templates of the LIGO-Virgo detection GW190521 [13] in Ref. [5] and to the 824 simulations included in the latest (fourth release [14]) Rochester Institute of Technology (RIT) catalog of binary black hole simulations. In Refs. [5,14], the initial eccentricity was then approximately evaluated by the Newtonian relationship $e = 2f - f^2$. In this paper, we extend this definition to higher post-Newtonian (PN) orders to improve the identification of highly eccentric simulations and to test it against full numerical evolutions.

II. METHOD

The idea of this method applied to PN expansions is to evaluate the conserved Hamiltonian at the two radial turning points of a binary $r_\pm$, to evaluate j, the conserved angular momentum at those points, and to relate the eccentric and circular values at the apastron r_+ by a factor $(1-f)$ as displayed in Fig. 1, following the equivalent of what we will perform for evaluating eccentricities for the full numerical simulations.

A. Nonspinning case

Let us begin with the nonspinning binary case, for which we can write the reduced Hamiltonian $\mathcal{H} = H/\mu$ with $\mu = m_1 m_2/(m_1+m_2)$,

$$\mathcal{H}(\mathbf{r},\hat{\mathbf{p}}) = \mathcal{H}_0(\mathbf{r},\hat{\mathbf{p}}) + \frac{1}{c^2}\mathcal{H}_1(\mathbf{r},\hat{\mathbf{p}}) + \frac{1}{c^4}\mathcal{H}_2(\mathbf{r},\hat{\mathbf{p}}) + \frac{1}{c^6}\mathcal{H}_3(\mathbf{r},\hat{\mathbf{p}}), \quad (1)$$

where explicit expressions for the reduced 3PN Hamiltonian in the ADMTT (Arnowit-Deser-Misner transverse traceless)

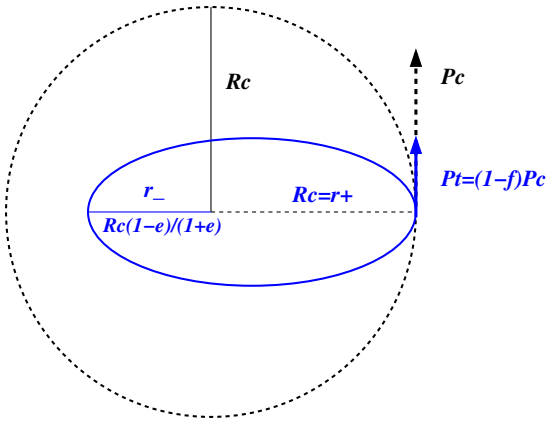

FIG. 1. Schematic of the initial momentum choice to describe eccentric orbits in our numerical relativity simulations. R_c and P_c denote the initial separation and tangential momentum for a quasicircular binary. Then, $P_t = (1-f)P_c$, where f is a fractional parameter, $0 \leq f \leq 1$, is the initial tangential momentum for an eccentric binary with an instantaneous eccentricity e. Here, one of the focus points (F1) of the ellipse is located at the center of the circle.

gauge that are given in Ref. [15] (see also Appendix A and Ref. [16] for a history on Hamiltonian results). Here, we define $\mathbf{r} = \mathbf{R}/(GM)$ and $\hat{\mathbf{p}} = \mathbf{P}/\mu$ where $\mathbf{R}$ is the relative separation vector, $M = m_1 + m_2$, and $\mathbf{P}$ is the linear momentum. Writing this Hamiltonian in polar coordinates (r, θ, ϕ), we see that it does not depend on the coordinate ϕ. Therefore, $\hat{p}_\phi$ is a conserved quantity and the motion will happen only on a plane. Thus, we may consider $\hat{\mathbf{p}} = (\hat{p}_r, 0, \hat{p}_\phi/r)$ at $\mathbf{r} = (r, 0, 0)$ in Cartesian coordinates (x, y, z). Now, $\hat{p}_r$ vanishes at the turning points r_+ and r_-, and we can write

$$\mathcal{H}(\mathbf{r}_\pm, \hat{\mathbf{p}}) = \mathcal{H}(r_\pm, \hat{p}_\phi) = \mathcal{H}_(r_\pm, j), \tag{2}$$

where $j = \hat{p}_\phi$ is constant along the orbit.

We now define the eccentricity measure e_r as

$$e_r = \frac{r_+ - r_-}{r_+ + r_-}. \tag{3}$$

Therefore, r_- is given by

$$r_- = r_+ \frac{1 - e_r}{1 + e_r} \tag{4}$$

(see Fig. 1 where $R_c = r_+$ and $e = e_r$).

To simplify more the computation, we scale again the Hamiltonian, the momentum $\hat{\mathbf{p}}$, and the r-coordinate as

$$\tilde{\mathcal{H}} = r_+ \mathcal{H}, \qquad \tilde{\mathbf{p}} = \sqrt{r_+}\hat{\mathbf{p}}, \qquad \tilde{\mathbf{r}} = \frac{\mathbf{r}}{r_+}. \tag{5}$$

This allows us to rewrite the Hamiltonian as

$$\tilde{\mathcal{H}}(\tilde{\mathbf{r}}, \tilde{\mathbf{p}}) = \tilde{\mathcal{H}}_0(\tilde{\mathbf{r}}, \tilde{\mathbf{p}}) + \alpha\tilde{\mathcal{H}}_1(\tilde{\mathbf{r}}, \tilde{\mathbf{p}}) + \alpha^2\tilde{\mathcal{H}}_2(\tilde{\mathbf{r}}, \tilde{\mathbf{p}}) + \alpha^3\tilde{\mathcal{H}}_3(\tilde{\mathbf{r}}, \tilde{\mathbf{p}}), \tag{6}$$

where $\alpha = 1/(c^2 r_+)$.

The advantage of this rescaling is that in this way we explicitly remove the value of r_+ from our problem. This appears only in the expression for α. In particular, we have (in polar coordinates)

$$\tilde{r}_+ = 1, \qquad \tilde{r}_- = \frac{1 - e_r}{1 + e_r}. \tag{7}$$

Now since the Hamiltonian is conserved along the orbit, we must have

$$\tilde{\mathcal{H}}(\tilde{r}_+, \tilde{j}) - \tilde{\mathcal{H}}(\tilde{r}_-, \tilde{j}) = 0, \tag{8}$$

where

$$\tilde{j} = \frac{j}{\sqrt{r_+}}. \tag{9}$$

Using Eqs. (7) and (8), and specifying values for α and η, we have an expression for $\tilde{j}$ in terms of e_r. Finally, introducing a momentum suppression factor f as

$$\tilde{j}(e_r) = (1 - f)\tilde{j}_C, \tag{10}$$

where $\tilde{j}(0) = \tilde{j}_C$ for the circular orbit, we obtain

$$f(e_r) = 1 - \frac{\tilde{j}(e_r)}{\tilde{j}_C}. \tag{11}$$

This final expression provides us with the desired relationship to evaluate $f(e_r)$ and to invert (numerically) for any specific set of initial parameters of a binary black hole simulation and obtain the estimated e_r (for example, see Appendix B for an implementation).

B. Spinning case

For the spinning case, we can apply the same method. Let us consider two orbiting black holes with spins $\mathbf{S}_1$ and $\mathbf{S}_2$. The Hamiltonian becomes [17,18] (we restore here the explicit dependence with the speed of light c to better display PN orders)

$$\mathcal{H}(\mathbf{r},\hat{\mathbf{p}},\mathbf{S}_1,\mathbf{S}_2) = \mathcal{H}_0(\mathbf{r},\hat{\mathbf{p}}) + \frac{1}{c^2}\mathcal{H}_1(\mathbf{r},\hat{\mathbf{p}}) + \frac{1}{c^4}\mathcal{H}_2(\mathbf{r},\hat{\mathbf{p}}) + \frac{1}{c^6}\mathcal{H}_3(\mathbf{r},\hat{\mathbf{p}}) + \frac{\delta}{c^2}\mathcal{H}^{\rm LO}_{\rm SO}(\mathbf{r},\hat{\mathbf{p}},\mathbf{S}_1,\mathbf{S}_2) + \frac{\delta}{c^4}\mathcal{H}^{\rm NLO}_{\rm SO}(\mathbf{r},\hat{\mathbf{p}},\mathbf{S}_1,\mathbf{S}_2) + \frac{\delta^2}{c^2}\mathcal{H}^{\rm LO}_{S1S2}(\mathbf{r},\hat{\mathbf{p}},\mathbf{S}_1,\mathbf{S}_2) + \frac{\delta^2}{c^2}\mathcal{H}^{\rm LO}_{S^2}(\mathbf{r},\hat{\mathbf{p}},\mathbf{S}_1,\mathbf{S}_2) + \frac{\delta^2}{c^4}\mathcal{H}^{\rm NLO}_{S1S2}(\mathbf{r},\hat{\mathbf{p}},\mathbf{S}_1,\mathbf{S}_2) + \frac{\delta^2}{c^4}\mathcal{H}^{\rm NLO}_{S^2}(\mathbf{r},\hat{\mathbf{p}},\mathbf{S}_1,\mathbf{S}_2) + \frac{\delta}{c^6}\mathcal{H}^{\rm NNLO}_{SO}(\mathbf{r},\hat{\mathbf{p}},\mathbf{S}_1,\mathbf{S}_2) + \frac{\delta^3}{c^4}\mathcal{H}^{\rm LO}_{S^3}(\mathbf{r},\hat{\mathbf{p}},\mathbf{S}_1,\mathbf{S}_2), \tag{12}$$

where δ is a dimensionless factor introduced to keep track of the spin order (linear, quadratic, or cubic) of the term considered (see also Ref. [17]). In this case, we define

$$\tilde{\mathbf{S}}_a = \frac{\mathbf{S}_a}{\sqrt{r_+}} = \sqrt{\alpha}\boldsymbol{\chi}_a, \qquad (a=1,2), \tag{13}$$

where in the last equality we introduced the dimensionless quantity $\boldsymbol{\chi}_a$ as

$$\boldsymbol{\chi}_a = \frac{\hat{\mathbf{S}}_a}{m_a^2}, \qquad (a=1,2). \tag{14}$$

Here, $\hat{\mathbf{S}}_a$ are the actual spins with dimension (geometric units) $[\hat{\mathbf{S}}] = [(\text{Mass})]^2$.

In terms of this new dimensionless variable, we have the rescaled Hamiltonian as

$$\tilde{\mathcal{H}}(\tilde{\mathbf{r}},\tilde{\mathbf{p}},\boldsymbol{\chi}_1,\boldsymbol{\chi}_2) = \tilde{\mathcal{H}}_0(\tilde{\mathbf{r}},\tilde{\mathbf{p}}) + \alpha\tilde{\mathcal{H}}_1(\tilde{\mathbf{r}},\tilde{\mathbf{p}}) + \alpha^2\tilde{\mathcal{H}}_2(\tilde{\mathbf{r}},\tilde{\mathbf{p}}) + \alpha^3\tilde{\mathcal{H}}_3(\tilde{\mathbf{r}},\tilde{\mathbf{p}}) + \alpha^{3/2}\tilde{\mathcal{H}}^{\rm LO}_{\rm SO}(\tilde{\mathbf{r}},\tilde{\mathbf{p}},\boldsymbol{\chi}_1,\boldsymbol{\chi}_2) + \alpha^{5/2}\tilde{\mathcal{H}}^{\rm NLO}_{\rm SO}(\tilde{\mathbf{r}},\tilde{\mathbf{p}},\boldsymbol{\chi}_1,\boldsymbol{\chi}_2) + \alpha^2\tilde{\mathcal{H}}^{\rm LO}_{S1S2}(\tilde{\mathbf{r}},\tilde{\mathbf{p}},\boldsymbol{\chi}_1,\boldsymbol{\chi}_2) + \alpha^2\tilde{\mathcal{H}}^{\rm LO}_{S^2}(\tilde{\mathbf{r}},\tilde{\mathbf{p}},\boldsymbol{\chi}_1,\boldsymbol{\chi}_2) + \alpha^3\tilde{\mathcal{H}}^{\rm NLO}_{S1S2}(\tilde{\mathbf{r}},\tilde{\mathbf{p}},\boldsymbol{\chi}_1,\boldsymbol{\chi}_2) + \alpha^3\tilde{\mathcal{H}}^{\rm NLO}_{S^2}(\tilde{\mathbf{r}},\tilde{\mathbf{p}},\boldsymbol{\chi}_1,\boldsymbol{\chi}_2) + \alpha^{7/2}\tilde{\mathcal{H}}^{\rm NNLO}_{\rm SO}(\tilde{\mathbf{r}},\tilde{\mathbf{p}},\boldsymbol{\chi}_1,\boldsymbol{\chi}_2) + \alpha^{7/2}\tilde{\mathcal{H}}^{\rm LO}_{S^3}(\tilde{\mathbf{r}},\tilde{\mathbf{p}},\boldsymbol{\chi}_1,\boldsymbol{\chi}_2). \tag{15}$$

We can now follow the same steps as indicated in Eqs. (8)–(11) to obtain a relationship between the fractional parameter f, by which the tangential circular momentum is suppressed to generate eccentric orbits, and the eccentricity e_r, defined through the periastron and apastron.

III. RESULTS

Here, we first validate our method to evaluate eccentricities at the periastron with actual post-Newtonian equation of motion integrations (3PN in the ADMTT gauge). We will then compare our method with full numerical simulations. In the applications below, we will assume, for the sake of definiteness and comparisons with the simulations used for GW190521 in Ref. [5], an initial coordinate separation of the holes of about $r \approx 24.7M$, which we use in the evaluation of α above. This corresponds in the cases studied in Ref. [5] to an initial quasicircular reference frequency of 10 Hz for a $M = 30\ \mathrm{M}_\odot$ system, as evaluated by the techniques described in Ref. [12]. We will also consider another application for unequal mass binaries starting at $r \approx 11.3M$. This range covers essentially all our simulations in the RIT catalog's initial separations [14].

A. Explicit analytic expressions for 1PN

Here, we derive explicit analytic expressions for $f(e_r)$ at a lower order PN expansions in the eccentricity. We hence consider the 1PN Hamiltonian,

$$H = \frac{1}{2}\frac{P_\phi{}^2}{r^2} - \frac{1}{r} + \alpha\left[\frac{1}{8}\frac{(3\eta-1)P_\phi{}^4}{r^4} - \frac{1}{2}\frac{(3+\eta)P_\phi{}^2}{r^3} + \frac{1}{2r^2}\right]. \tag{16}$$

From equating the values of the Hamiltonian at the periastron and apastron r_+,

$$H(r=r_+,P_\phi^2) = H(r=r_+(1-e_r)/(1+e_r),P_\phi^2), \tag{17}$$

picking up the right root of P_ϕ^2, we find an analytic expression for $f(e_r) = 1 - \sqrt{P_\phi^2/P_\phi^2(e_r=0)}$ at 1PN,

$$f(e_r) = 1 - \left\{\frac{(1-e)}{(e^2+1)(\sqrt{\Delta+4}+3\alpha(\eta+3)-2)}[3\alpha(\eta+3)+\alpha e^2(\eta+3)+(\Delta+\alpha^2e^4(\eta+3)^2-20\alpha e^3(\eta-1) + 2e^2(\alpha(\alpha(3\eta(\eta+2)+31)+10(\eta-1))+2)-4e(3\alpha\eta-11\alpha+2)+4)^{1/2}+2e-2]\right\}^{1/2}, \tag{18}$$

where

$$\Delta = \alpha(\alpha(9\eta^2 + 30\eta + 89) + 12\eta - 44). \quad (19)$$

We can find an approximate expression for $f(e_r)$ expanding in powers of α to obtain

$$f(e_r) = 1 - \sqrt{1-e_r} + \frac{e_r(-4 + e_r(-2+\eta))}{2\sqrt{1-e_r}}\alpha. \quad (20)$$

This expression can be used as a first estimate up to intermediate eccentricities, $e_r < 0.6$ in the large separation regime $r_+ > 12M$, comparable masses $q > 1/4$, and slowly spinning black holes $\chi_i < 0.5$, as we verified by direct comparisons with full 3PN expressions in Fig. 2, representing the first correction to the Newtonian estimate used in the fourth RIT binary black holes waveforms catalog [14] and the analysis of GW190521 [5]. The advantage of using the full expressions, particularly at higher PN orders, relies on the behavior at large e_r and the merging of curves toward the expected limit $f(e_r = 1) = 1$.

B. $f(e_r)$ for initial parameters and its comparison with integrations of 3PN equations of motion

The result for nonspinning equal mass binaries, i.e., the mass ratio $q = m_2/m_1 = 1$, at different successive PN orders is shown in Fig. 2. We plot here the factor f by which we reduce the tangential linear momentum of a quasicircular orbit versus the computed eccentricity e_r. This allows us to read off the eccentricity associated with our initial data setup (here at $r = 24M$ for reference). We can see the good agreement to all displayed PN orders at low eccentricities ($e_r < 0.4$). At intermediate eccentricities, the 1PN computation deviates from the higher order trend for $e_r > 0.4$, while the 2PN computation remains consistent for $e_r < 0.7$. On the other hand, the 3PN computation converges toward the Newtonian (0PN) curve for larger e_r. We interpret this as the correct behavior since for large e_r the expected evolution of a binary is essentially a plunge that tends to reduce the differences between PN orders.

In the case of spinning holes, we will hence focus directly on the 3PN computation and compare them with the nonspinning case. To better display the effects (and the subsequent comparisons with full numerics), we consider the cases when both equal mass black holes have spins aligned ($\chi_i = +0.8$) or antialigned ($\chi_i = -0.8$) with the orbital angular momentum (we checked that the $\chi_1 = -\chi_2$ case gives a curve remarkably close to the nonspinning case). The results for this 3PN order comparison for the various values of the spins are shown in Fig. 3 (note that the dashed lines for the corresponding 3PN equations of motion integration are truncated as they lead to mergers at large e). We observe a close dependence of the three curves for small and intermediate eccentricities, but for $e_r > 0.75$ there is a reverse in their relative behavior. While the case of aligned spins eventually merges for large eccentricities (plunges) with the nonspinning holes, the antialigned spins case shows a quite different behavior. We will come back later to this case with a 3.5PN computation that resolves this behavior.

A first validation of our initial instantaneous eccentricity estimate can be performed by comparing our analytical results with the numerical integrations of the conservative 3PN equation of motion [19,20], where we suppressed the 2.5PN radiative terms. We integrate the orbital motion over the first orbit and evaluate the eccentricity from the apastron and periastron differences, $e_r = (r_+ - r_-)/(r_+ + r_-)$. The comparisons for spinning and nonspinning cases with $q = 1$ and $\chi_i = 0, \pm 0.8$ are displayed in Fig. 3. The results show a

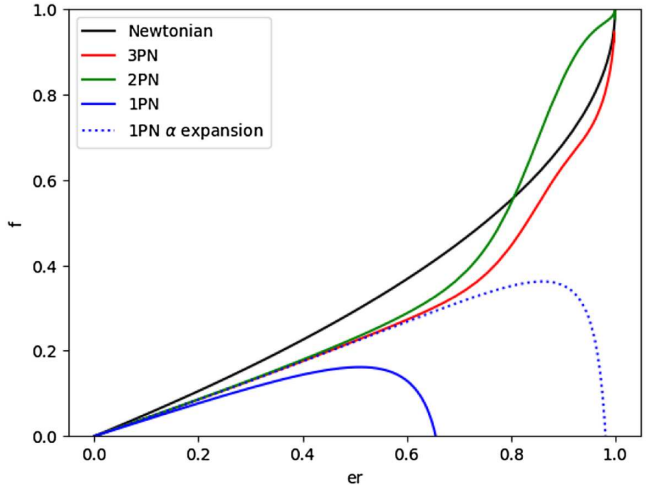

FIG. 2. Momentum suppression factor f vs eccentricity e_r for nonspinning equal mass binaries, $\chi_i = 0$ and $q = 1$, at various PN orders. Dotted lines are for the first order α-expansions of the 1PN calculation.

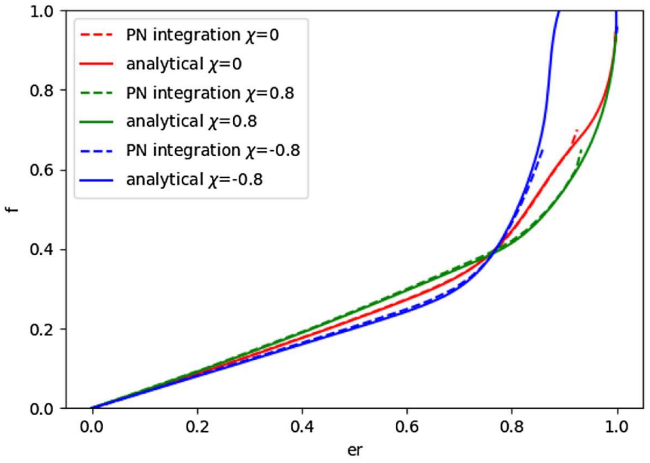

FIG. 3. Comparison of initial analytic vs integration of the 3PN equations of motion: Eccentricity e_r vs momentum suppression factor f for $q = 1$ and different values of the spins.

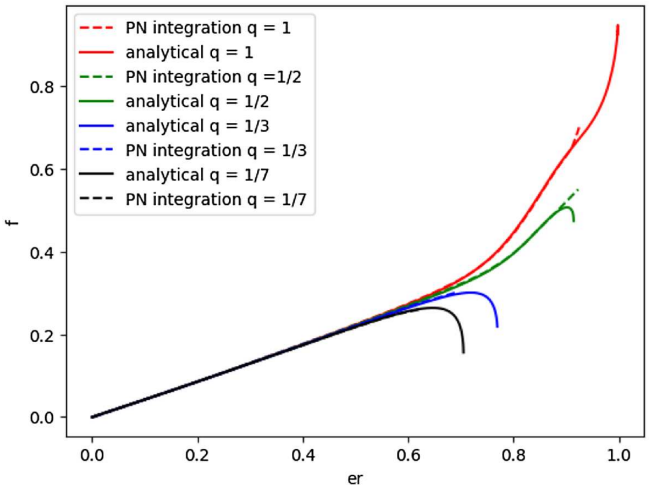

FIG. 4. Comparison of initial analytic vs 3PN equation of motion integration of the momentum suppression factor f vs eccentricity e_r for nonspinning binaries, $\chi_i = 0$, and different values of the mass ratio q.

TABLE I. Eccentric simulations used in Fig. 5 and their estimated eccentricities from its radial turning points e_r^{NR}. Here, R_c denotes the initial separation, q, χ_1^z, and χ_2^z are the mass ratio and the dimensionless spins projected along the initial orbital angular momentum, respectively, and f is the momentum suppression factor.

RIT catalog no.	R_c	q	χ_1^z	χ_2^z	f	e_r^{NR}
RIT:eBBH:1282	24.64	1	0.0	0.0	0.10	0.2357
RIT:eBBH:1283	24.64	1	0.0	0.0	0.15	0.3416
RIT:eBBH:1285	24.64	1	0.0	0.0	0.20	0.4459
RIT:eBBH:1293	24.64	1	0.0	0.0	0.25	0.5488
RIT:eBBH:1303	24.64	1	0.0	0.0	0.30	0.6646
RIT:eBBH:1807	24.56	1	0.8	0.8	0.25	0.5064
RIT:eBBH:1808	24.56	1	0.8	0.8	0.27	0.5410
RIT:eBBH:1809	24.56	1	0.8	0.8	0.30	0.5915
RIT:eBBH:1811	24.56	1	0.8	0.8	0.35	0.6735
RIT:eBBH:1813	24.56	1	0.8	0.8	0.40	0.7587
RIT:eBBH:1763	24.75	1	−0.8	−0.8	0.10	0.2644
RIT:eBBH:1764	24.75	1	−0.8	−0.8	0.20	0.5143

notable agreement and consistency between the integrated and initial estimates of the eccentricity, for $e_r \leq 0.9$, at 3PN order.

To verify the mass ratio dependence of our eccentricity estimator as well, we compare our analytical results with numerical evolutions of the 3PN equations of motion in Fig. 4 for mass ratios $q = 1, 1/2, 1/3$, and $1/7$ (for nonspinning binaries). We observe again a notable agreement in their corresponding regions of validity (as the 3PN approximation reduces its validity to medium and small eccentricity as we deal with smaller mass ratios).

C. Comparisons with full numerical relativity simulations

We are now able to directly compare our initial eccentricity PN estimates to actual full numerical simulations where it is possible to evaluate the eccentricity via the turning points in the simulations. We thus identify the numerical and PN (in the ADMTT gauge) parameters, $R_c = r_+$ and $P_c = P_\phi(e_r = 0)/r_+$, and the values of f, α, q, and S_1 and S_2 for several simulations available in the RIT waveforms catalog [14] identified in Table I. The results are displayed in Fig. 5. The agreement for simulations in the range of low to middle eccentricities is remarkable. We also include here the 3.5PN corrections to the antialigned spins configurations to display an improved behavior all the way up to $e_r \to 1$, merging with the plunging behavior in the cases of nonspinning and aligned spins.

In the RIT catalog [14], we have another family of eccentric simulations (for nonspinning and different mass ratios $q = 1, 3/4, 1/2$, and $1/4$), starting at much closer initial separations, $r \approx 11.35M$, that we can use to compare to our PN eccentric estimations. These separations are roughly half the ones we considered so far and are at the limit of applicability of PN expansions. The results of these estimates are displayed in Fig. 6. It is also difficult to compute the e_r from the full numerical evolutions for large eccentricities since the trajectories are highly inspiral or merge before we can complete a meaningful orbit to extract r_+ and r_-. Yet, the estimates are very good for the expected range of validity of the PN expansions for small mass ratios (here $e_r < 0.5$). The excellent agreement between the analytic and full numerical estimates extends to the intermediate mass ratio $q = 1/7$ when we consider

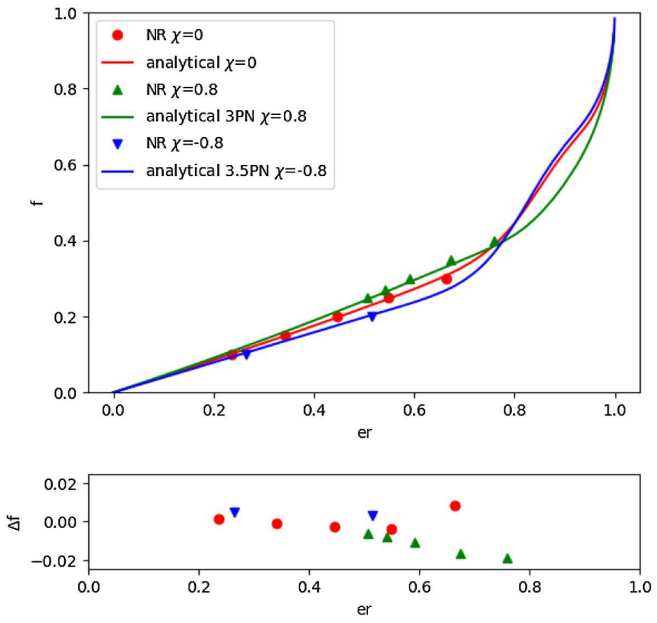

FIG. 5. Top: momentum suppression factor f vs eccentricity e_r with PN estimates for various spins (continuous curves) in comparison with the full numerical simulation measurements (dots). Bottom: differences between the PN and numerical values.

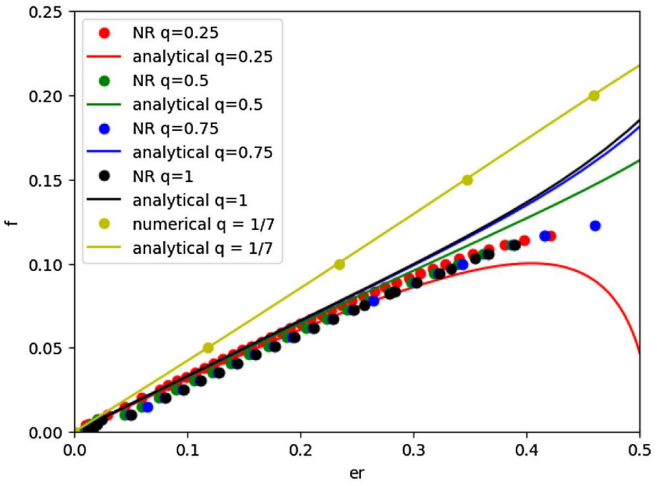

FIG. 6. Momentum suppression factor f vs eccentricity e_r for various mass ratio nonspinning binaries using 3PN estimates (continuous curves) at $r = 11.35M$, in comparison with the corresponding full numerical simulations evaluations (dots). The $q = 1/7$ case is taken at initial separation $r = 24.7M$ to display the improved agreement with larger r.

the larger initial separation $r = 24.7M$ at the apastron, showing the convergence of the PN approach at larger separations.

We conclude that our eccentricity estimator provides an accurate description of the initial eccentric properties for binary black holes and can be directly applied to all the eccentric simulations in the fourth RIT catalog [14] and future targeted studies.

IV. CONCLUSIONS AND DISCUSSION

We have defined eccentric binary black hole simulations invariantly in terms of fractional, $f = 1 - P_t(e_r)/P_c$, tangential linear momenta to the circular one. We have found that the PN analytic estimates of the initial eccentricity of these full numerical simulations are an accurate and practical tool to predict and assess the eccentricity of the first orbit in full numerical simulations, allowing, for instance, precise design of new runs for parameter coverage or targeted studies. For low and medium eccentricities, $e_r < 0.5$, and separated enough binaries [see also Eq. (20) for the 1PN analytic expression], even the 2PN estimates are accurate (see Appendixes A and B for an explicit implementation). For higher eccentricities and highly spinning (particularly for both antialigned) binary black holes, we require the 3PN, 3.5PN, or even eventually 4PN estimates at closer initial separations and higher eccentricities, i.e., $e_r \sim 0.85$ [21]. Our formalism can be also applied to generic orientations of the spins by use of the concept of spherical orbits [22] to compute the turning points $r_\pm$.

Here, we have suppressed the tangential momentum with respect to the quasicircular one by a $(1 - f)$ factor, with $0 \leq f \leq 1$. But if we allow for $f < 0$, we would actually increase the tangential momentum, leading to an elliptic orbit, but starting at the periastron (r_-) instead of the apastron (r_+). This can be evaluated by reversing the sign of e in our equations. For instance, for the Newtonian case we would have $e_r = -2f + f^2$ and for $F_p < f \leq 0$, where in this case $F_p = 1 - \sqrt{2} = -0.41421356$, would lead to a parabola. For values more negative than this F_p, i.e., $f < F_p$, we would generate a hyperbolic orbit.

The estimates which we have developed can now be directly applied to the 824 eccentric simulations in the fourth RIT catalog [14]. Our formulas should still provide good estimates for well-separated precessing binaries with small radial momentum components by use of the projected spins along the initial orbital angular momentum as variables. This is the case for all our simulations in Ref. [14], and in particular, we can now reassess the best eccentricity estimate of the gravitational wave event GW190521 [5]. In that paper, we assessed the eccentricity of the optimal full numerical simulation (precessing binary, with in-plane spin components $\chi^p_{1,2} = 0.66$, aligned spin components $\chi^z_{1,2} = 0.27$, $q = 1$, $R_c = 24.7M$, and $f = 0.44$) with the Newtonian estimate to be $e_N = 0.69$. We can now recompute the eccentricity using our 3.5PN estimator by evaluating the turning points $r_\pm$, assuming that in the first half orbit negligible precession of the spins took place, and find $e_{\rm PN} = 0.80$, which highlights again the potentially interesting astrophysical scenarios that might have led to the merger of the two black holes generating GW190521 [23,24].

ACKNOWLEDGMENTS

The authors gratefully acknowledge the National Science Foundation (NSF) for financial support from Grant No. PHY-1912632. Computational resources were also provided by the NewHorizons, BlueSky Clusters, GreenPrairies, and WhiteLagoon at the Rochester Institute of Technology, which were supported by NSF Grants No. PH-0722703, No. DMS-0820923, No. AST-1028087, No. PHY-1229173, No. PH-1726215, and No. PH-2018420. This work used the Extreme Science and Engineering Discovery Environment (XSEDE) [allocation TG-PHY060027N], which is supported by NSF Grant No. ACI-1548562 and project PHY20007 Frontera, an NSF-funded petascale computing system at the Texas Advanced Computing Center (TACC). H. N. is supported by JSPS/MEXT KAKENHI Grants No. JP21K03582, No. JP21H01082, and No. JP17H06358.

APPENDIX A: PN HAMILTONIAN

In this appendix we provide the explicit form of the Hamiltonian terms (up to 2PN order) that we used throughout this paper. From Eq. (7) in Ref. [15] (see also Refs. [25,26] for the 1PN equations of motion and Refs. [27–33] for the 2PN Hamiltonian) in the ADMTT gauge that is closer to our gauge choice in the numerical simulations [34], we have the nonspinning components of the Hamiltonian,

$$\mathcal{H}_0(\mathbf{r},\hat{\mathbf{p}}) = \frac{\hat{\mathbf{p}}^2}{2} - \frac{1}{r}, \tag{A1}$$

$$\mathcal{H}_1(\mathbf{r},\hat{\mathbf{p}}) = \frac{1}{8}(3\eta-1)(\hat{\mathbf{p}}^2)^2 - \frac{1}{2r}[(3+\eta)\hat{\mathbf{p}}^2 + \eta(\mathbf{n}\cdot\hat{\mathbf{p}})^2] + \frac{1}{2r^2}, \tag{A2}$$

$$\begin{aligned}\mathcal{H}_2(\mathbf{r},\hat{\mathbf{p}}) = {}& \frac{1}{16}(1-5\eta+5\eta^2)(\hat{\mathbf{p}}^2)^3 + \frac{1}{8r}[(5-20\eta-3\eta^2)(\hat{\mathbf{p}}^2)^2 - 2\eta^2(\mathbf{n}\cdot\hat{\mathbf{p}})^2\hat{\mathbf{p}}^2 - 3\eta^2(\mathbf{n}\cdot\hat{\mathbf{p}})^4] \\ & + \frac{1}{2r^2}[(5+8\eta)\hat{\mathbf{p}}^2 + 3\eta(\mathbf{n}\cdot\hat{\mathbf{p}})^2] - \frac{1}{4r^3}(1+3\eta),\end{aligned} \tag{A3}$$

where $\eta = m_1 m_2/(m_1+m_2)^2$.

The explicit expressions for the spin terms of the Hamiltonian are given in Eqs. (13)–(16) of Ref. [17] and Eqs. (15)–(18) of Ref. [18]. Here, we write some of them in the notation used throughout this paper,

$$\mathcal{H}^{\mathrm{LO}}_{\mathrm{SO}}(\mathbf{r},\hat{\mathbf{p}},\mathbf{S}_1,\mathbf{S}_2) = \frac{1}{r^3}\left[\left(1-\frac{\eta}{2}+\sqrt{1-4\eta}\right)(\mathbf{h}\cdot\mathbf{S}_1) + \left(1-\frac{\eta}{2}-\sqrt{1-4\eta}\right)(\mathbf{h}\cdot\mathbf{S}_2)\right], \tag{A4}$$

$$\mathcal{H}^{\mathrm{LO}}_{S^2}(\mathbf{r},\hat{\mathbf{p}},\mathbf{S}_1,\mathbf{S}_2) = \frac{\eta}{r^3}[\lambda_1(-1+2\eta-\sqrt{1-4\eta})(3(\mathbf{n}_{12}\cdot\mathbf{S}_1)^2-(\mathbf{S}_1\cdot\mathbf{S}_1)) + \lambda_2(-1+2\eta+\sqrt{1-4\eta})(3(\mathbf{n}_{12}\cdot\mathbf{S}_2)^2-(\mathbf{S}_2\cdot\mathbf{S}_2))], \tag{A5}$$

$$\mathcal{H}^{\mathrm{LO}}_{S1S2}(\mathbf{r},\hat{\mathbf{p}},\mathbf{S}_1,\mathbf{S}_2) = \frac{\eta}{r^3}(3(\mathbf{n}_{12}\cdot\mathbf{S}_1)(\mathbf{n}_{12}\cdot\mathbf{S}_2) - (\mathbf{S}_1\cdot\mathbf{S}_2)), \tag{A6}$$

where for BHs $\lambda_1 = \lambda_2 = -1/2$, $\mathbf{n}_{12} = \mathbf{r}/|r|$ and $\mathbf{h} = r\mathbf{n}_{12}\times\hat{\mathbf{p}}$.

APPENDIX B: SCRIPTS/NOTEBOOKS

Here, in Fig. 7, we present a minimalistic script to compute the eccentricity from the full numerical simulation parameters q, R, χ_1^z, χ_2^z, and f. For the sake of simplicity, we only include explicitly up to the 2PN Hamiltonian terms (see Ref. [35] and references therein), but in the results of the paper we computed up to 3.5PN terms. 4PN local terms can be added in a straightforward way too, but the nonlocal terms (see Ref. [16]) are more difficult to include in our formalism. The script only allows for spins oriented along the z-axis but it can be extended in order to include any orientation of the spins.

2 | 2PN_tpm_script.wls

```
#/usr/local/bin/wolframscript

If[Length[$ScriptCommandLine] < 6, Print["\nNot enough arguments.
The argument format
    is:\n\nmass_ratio GM/(r*c^2) Spin_mass_1 Spin_mass_2 f "];
 Quit[]]

H0 = P^2/2 - 1/r;
H1 = (3η-1) P^4/8 - 1/(2r) (3+η) P^2 + 1/(2r^2);
HSOLO = P/(r^2) ((1-η/2 + Sqrt[1-4η]) S1 + (1-η/2 - Sqrt[1-4η]) S2);
H2 = (1-5η+5η^2)/16 P^6 + 1/(8r) (5-20η-3η^2) P^4 +
   1/(2r^2) (5+8η) P^2 - 1/(4r^3) (1+3η);
HS1S2LO = η/(r^3) (-S1 S2);
HS2LO =
  1/(2r^3) (-λ1 (-1+2η-Sqrt[1-4η]) S1 S1 - λ2 (-1+2η+Sqrt[1-4η]) S2 S2);
HSONLO = 0;
H3 = 0;
HS1S2NLO = 0;
HS2NLO = 0;
HSONNLO = 0;
HS3LO = 0;

Clear[Pphi, PphiC, f];

P = Pphi/r;

q = ToExpression[$ScriptCommandLine[2]];
η = Rationalize[q/(1+q)^2];
α = Rationalize[ToExpression[$ScriptCommandLine[3]]];
S1 = Rationalize[ToExpression[$ScriptCommandLine[4]]];
S2 = Rationalize[ToExpression[$ScriptCommandLine[5]]];
λ1 = -1/2;
λ2 = -1/2;
CQ1 = 1;
CQ2 = 1;

H = H0 + α H1 + α^(3/2) HSOLO + α^2 (HS1S2LO + HS2LO + H2) + α^(5/2) (HSONLO) +
α^3 (H3 + HS1S2NLO + HS2NLO) + α^(7/2) (HSONNLO + HS3LO);

s = Solve[(D[H, r] r^5 /. r → 1) == 0, Pphi];

PphiC = Select[
   Select[N[s[[All, 1, 2]]], Abs[Im[#]] < 10^(-13) &], Re[#] ≥ 1 && Re[#] < 2 &][[1]

ra = 1;
rp = (1-e)/(1+e);

Hp = (H /. r → rp);

Ha = (H /. r → ra);

s2 = Solve[(Ha - Hp) (1-e)^6/e == 0, Pphi];

Pphi = s2[[Position[N[s2[[All, 1, 2]] /. e → 0],
       Select[Select[N[s2[[All, 1, 2]] /. e → 0],
Abs[Im[#]] < 10^(-13) &], Re[#] ≥ 1 && Re[#] < 2 &][[1]]][[1, 1]], 1, 2]];

N[Pphi /. e → 0]

f = ToExpression[$ScriptCommandLine[6]]

If[TimeConstrained[NSolve[1 - Pphi/PphiC == f, e][[1, 1, 2]], 20., 0] == 0 ||
  NSolve[1 - Pphi/PphiC == f, e] == {},
Print["The f value inserted does not give a solution for the PNOrder chosen"],
 Print[NSolve[1 - Pphi/PphiC == f, e][[1, 1, 2]]]

f = 1 - Pphi/PphiC;
```

FIG. 7. Script to evaluate the eccentricity (explicit to 2PN order).

[1] I. Hinder, L. E. Kidder, and H. P. Pfeiffer, Phys. Rev. D **98**, 044015 (2018).
[2] B. Ireland, O. Birnholtz, H. Nakano, E. West, and M. Campanelli, Phys. Rev. D **100**, 024015 (2019).
[3] A. Ramos-Buades, S. Husa, G. Pratten, H. Estellés, C. García-Quirós, M. Mateu-Lucena, M. Colleoni, and R. Jaume, Phys. Rev. D **101**, 083015 (2020).
[4] I. M. Romero-Shaw, P. D. Lasky, E. Thrane, and J. C. Bustillo, Astrophys. J. Lett. **903**, L5 (2020).
[5] V. Gayathri, J. Healy, J. Lange, B. O'Brien, M. Szczepanczyk, I. Bartos, M. Campanelli, S. Klimenko, C. O. Lousto, and R. O'Shaughnessy, Nat. Astron. **6**, 344 (2022).
[6] I. M. Romero-Shaw, P. D. Lasky, and E. Thrane, arXiv:2206.14695.
[7] A. Bonino, R. Gamba, P. Schmidt, A. Nagar, G. Pratten, M. Breschi, P. Rettegno, and S. Bernuzzi, arXiv:2207.10474.
[8] H. L. Iglesias *et al.*, arXiv:2208.01766.
[9] M. Campanelli, C. O. Lousto, P. Marronetti, and Y. Zlochower, Phys. Rev. Lett. **96**, 111101 (2006).
[10] S. Brandt and B. Brügmann, Phys. Rev. Lett. **78**, 3606 (1997).
[11] M. Ansorg, B. Brügmann, and W. Tichy, Phys. Rev. D **70**, 064011 (2004).
[12] J. Healy, C. O. Lousto, H. Nakano, and Y. Zlochower, Classical Quantum Gravity **34**, 145011 (2017).
[13] R. Abbott *et al.*, Phys. Rev. Lett. **125**, 101102 (2020).
[14] J. Healy and C. O. Lousto, Phys. Rev. D **105**, 124010 (2022).
[15] R.-M. Memmesheimer, A. Gopakumar, and G. Schaefer, Phys. Rev. D **70**, 104011 (2004).
[16] G. Schäfer and P. Jaranowski, Living Rev. Relativity **21**, 7 (2018).
[17] M. Tessmer, J. Hartung, and G. Schafer, Classical Quantum Gravity **27**, 165005 (2010).
[18] M. Tessmer, J. Hartung, and G. Schafer, Classical Quantum Gravity **30**, 015007 (2013).
[19] T. Damour, P. Jaranowski, and G. Schafer, Phys. Rev. D **77**, 064032 (2008).
[20] A. Buonanno, Y. Chen, and T. Damour, Phys. Rev. D **74**, 104005 (2006).
[21] G. Cho, S. Tanay, A. Gopakumar, and H. M. Lee, Phys. Rev. D **105**, 064010 (2022).
[22] A. Buonanno, L. E. Kidder, A. H. Mroue, H. P. Pfeiffer, and A. Taracchini, Phys. Rev. D **83**, 104034 (2011).
[23] R. Abbott *et al.* (LIGO Scientific, Virgo Collaborations), Astrophys. J. Lett. **900**, L13 (2020).
[24] O. Barrera and I. Bartos, Astrophys. J. Lett. **929**, L1 (2022).
[25] H. A. Lorentz and J. Droste, The motion of a system of bodies under the influence of their mutual attraction, according to Einstein's theory, in *Collected Papers: Volume V* (Springer Netherlands, Dordrecht, 1937), pp. 330–355.

[26] A. Einstein, L. Infeld, and B. Hoffmann, Ann. Math. **39**, 65 (1938).
[27] T. Ohta, H. Okamura, T. Kimura, and K. Hiida, Prog. Theor. Phys. **50**, 492 (1973).
[28] T. Ohta, H. Okamura, T. Kimura, and K. Hiida, Prog. Theor. Phys. **51**, 1598 (1974).
[29] T. Ohta, H. Okamura, K. Hiida, and T. Kimura, Prog. Theor. Phys. **51**, 1220 (1974).
[30] T. Damour and G. Schäfer, Gen. Relativ. Gravit. **17**, 879 (1985).
[31] G. Schaefer, Ann. Phys. (N.Y.) **161**, 81 (1985).
[32] G. Schäfer, Gen. Relativ. Gravit. **18**, 255 (1986).
[33] G. Schäfer, Phys. Lett. A **123**, 336 (1987).
[34] J. R. van Meter, J. G. Baker, M. Koppitz, and D.-I. Choi, Phys. Rev. D **73**, 124011 (2006).
[35] T. Damour, P. Jaranowski, and G. Schaefer, Phys. Rev. D **62**, 021501 (2000); **63**, 029903(E) (2000).